Mechanical Mapping and Morphology Across the Length Scales Unveil Structure–Property Relationships in Polycaprolactone Based Polyurethanes

Hubert Gojzewski,[1] Balazs Imre,[2] Casey Check,[3] Richard Chartoff,[2] Julius Vancso[1]

[1]Materials Science and Technology of Polymers, Faculty of Science and Technology, University of Twente, Enschede, 7522 NB, The Netherlands
[2]School of Chemical, Biological and Environmental Engineering, Oregon State University, Corvallis, Oregon, 97331
[3]Center for Advanced Materials Characterization in Oregon (CAMCOR), University of Oregon, Eugene, Oregon, 97405
Correspondence to: J. Vancso (E-mail: g.j.vancso@utwente.nl) or R. Chartoff (E-mail: chartofr@oregonstate.edu)

Received 25 May 2016; accepted 14 July 2016; published online 10 August 2016
DOI: 10.1002/polb.24140

ABSTRACT: Segmented polyurethane elastomers for biomedical applications were synthesized and studied at macroscopic (by mechanical testing) and meso/nanoscopic length scales (by atomic force microscopy, AFM). The polyurethanes are composed of 4,4′-methylenebis(phenyl isocyanate), 1,4-butanediol and an ε-polycaprolactone diol. The stoichiometric ratio of the isocyanate and hydroxyl groups is constant, but the polymer diol to total diol—varies from 0 to 100 %. We show the representative features of the morphology from phase separation to mixed phases, how this is related to the mechanical properties in the bulk and locally, at exposed free surfaces and at the nanoscale. We propose a morphological model considering the molecular structure, the length of hard segments, and the dimensions of both the soft and the hard phases, respectively. Understanding such structure–property relations is pivotal to establishing designer materials and controlling the performance of the final product to achieve optimal properties in polyurethane based medical devices. © 2016 Wiley Periodicals, Inc. J. Polym. Sci., Part B: Polym. Phys. **2016**, *54*, 2298–2310

KEYWORDS: atomic force microscopy (AFM); polyurethanes; morphology; nanoscale mechanical properties; adhesion; indentation; phase separation

INTRODUCTION Polyurethanes (PU) as engineering materials have been utilized in an impressive array of applications, including coatings, foams and synthetic leathers, as well as for the modification of other polymers.[1–4] In view of the very broad variety of the primary chemical structures, the supramolecular structure and morphology across the length scales (nanometer—millimeter domains), and thus the end-use properties of PUs, like stiffness, hardness, adhesion, and permeability vary over a wide range. Designer polyurethanes with fine-tuned properties can be obtained on the basis of the understanding of such structure–property relationships. Thus, the optimum design of the molecular structure and morphology must be the focus of interest for producing novel materials.

Segmented polyurethanes are multiblock copolymers that consist of alternating soft and hard chain segments that are separated in a complex fashion.[1,2,5–8] The morphology model we use in this study is shown in Scheme 1. Soft segments are often composed of oligomeric or polymeric diols with flexible chains that have subambient glass transition temperatures in their respective bulk forms, and usually consist of polyethers, polyesters, or polycarbonates (shown as wavy lines in Scheme 1). The hard segments (with relatively high glass transition temperatures) form by reactions of aromatic or aliphatic diisocyanates and low molar mass diols (or amines in the case of polyureas) (shown as rectangles and short connecting lines, between them, respectively, in Scheme 1). The low molar mass diols are referred to as chain extenders. The variation of the interaction between soft and hard segments, their relative amount, chemical structure, as well as their respective molar masses, determine the extent of phase separation, and thus the physicochemical properties of the final polymer.[1,6] Varying block length and chain composition offers unique possibilities to form tailor-made polymers.[2,8,9]

The structural diversity of PU chains results in a broad range of intermolecular interaction strengths.[2,6,10] As indicated by Król, hydrogen bonding is the strongest among these intermolecular forces, often contributing to the aggregation of the

Additional Supporting Information may be found in the online version of this article.

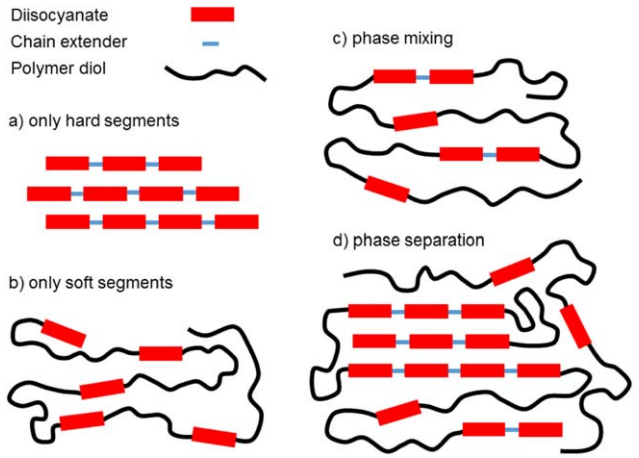

SCHEME 1 Schematic of the possible morphologies of segmented PUs: (a) PU consisting only of hard segments, (b) PU consisting only of soft segments, (c) hard segments dissolved in the soft phase, (d) separated soft and hard phase. [Color figure can be viewed in the online issue, which is available at wileyonlinelibrary.com.]

hard segments and to the formation of a compact rigid phase.[1] The rigid phase is typically only partially miscible with the less polar soft segments. As the hard segment concentration increases, thermodynamic immiscibility between the hard and the soft segments induces phase separation and a two-phase morphology is formed.[2] The studies of Kang and Stoffer showed that thermodynamic factors are more decisive than kinetic ones in affecting phase separation.[11] Thus, PUs with aliphatic hard segments have a more phase separated structure than their aromatic counterparts, that is, a lesser amount of hard segments dissolved in the soft phase, despite the higher mobility of their chains.[12]

The phase behavior in PUs is the key to controlling the performance of the final product.[1,2,9,10,13] To achieve the material composition best serving target applications, the structural elements of the material must be quantitatively characterized for a complete interpretation of the morphology and its macromolecular structure. Several attempts have been made to characterize the structural units (phase) of polyurethanes by mechanical contact tests (micro or nanoindentation).[14,15] However, even for nanoindentation where a tip is pressed against the surface and penetrates the material, the indentation depth has magnitudes on the order of hundreds of nanometers, resulting in "averaging" of the measured mechanical properties over a relatively large contact area (typically beyond tens of hundreds of μm^2). To overcome this averaging problem, atomic force microscopy (AFM) has been introduced with its sharp tip to perform indentation at the nanoscale (based on force spectroscopy and collecting the related force-distance curves).[16,17] The extension of this method was later automated and classified as a separate method, called a Force Volume mode.[16] Both methods are known to provide quantitative mechanical information about polymer surfaces, when additionally supported by mechanical contact models to derive elastic modulus values.[16,18,19] Schön et al. pointed out that these AFM methods, however, suffer due to limitation of the resolution and the significant capturing time required to obtain the mechanical property maps.[7] It is also of high importance to compare results obtained by nanoscale methods with other micro and macroscopic methods to reveal quantitative properties across the length scales. Such comparison is often discounted in the scientific reports.

Recently, several new AFM modes have been introduced with interesting quantitative modulus imaging possibilities. These include HarmoniX® (Bruker), PeakForce QNM® (Bruker), and QI™ (JPK Instruments AG, Germany).[7,20–24] All of these imaging modes are based on collecting force-distance curves followed by an on- or off-line analysis. Among them, PeakForce QNM is highlighted in this work due to its high resolution (<5 nm), high imaging speed (comparable to tapping mode), and a broad, accessible range of elastic moduli that can be quantitatively determined (0.7 MPa – 70 GPa), using a controlled load (feedback loop). It has been shown that the elastic modulus, as obtained by the PeakForce QNM mode, provides good quantitative agreement with other mechanical testing methods.[7,23]

There are only a very limited number of reports available on the applications of PeakForce QNM for the characterization of polyurethanes. In view of the high utilization potential of this technique, in particular for polyurethanes, there is a strong need for additional work. Schön et al. were the first to show the potential of the method for the determination of mechanical properties in polyurethanes.[7] Similar work was done by Imre et al.,[4] as well as Dokukin and Sokolov.[22] Recently, Fernandez-d'Arlas and Eceiza reported on the nanoscale elastic modulus in high urethane concentration polyurethanes.[25]

Numerous studies are available on polycaprolactone based polyurethanes and on their applications, in the medical field.[26] However most of them only apply indirect methods at best in order to characterize structure,[27–32] while only a handful attempt to use more direct imaging techniques such as AFM.[9,33–35] At this point we have to emphasize the fact that achieving a polyurethane material with desirable properties that meets the extremely demanding requirements of medical applications is not at all trivial. High elasticity, toughness and biocompatibility are important requirements to meet biomedical applicability.[26,36,37] The PUs are generally not in thermodynamic equilibrium following processing, and the mechanical behavior of the chosen class of PUs is hardly predictable.[1,2,10] Only the rigorous knowledge of structure–property relations can lead to the establishment of proper design criteria of the molecular structure in PUs to fulfil the mechanical requirements needed.

In this study, we aim at producing and characterizing PU elastomer based. We applied a combined approach including surface nanoscale mapping of mechanical performance and morphology with bulk studies to assess the relationship between structure and performance across the relevant

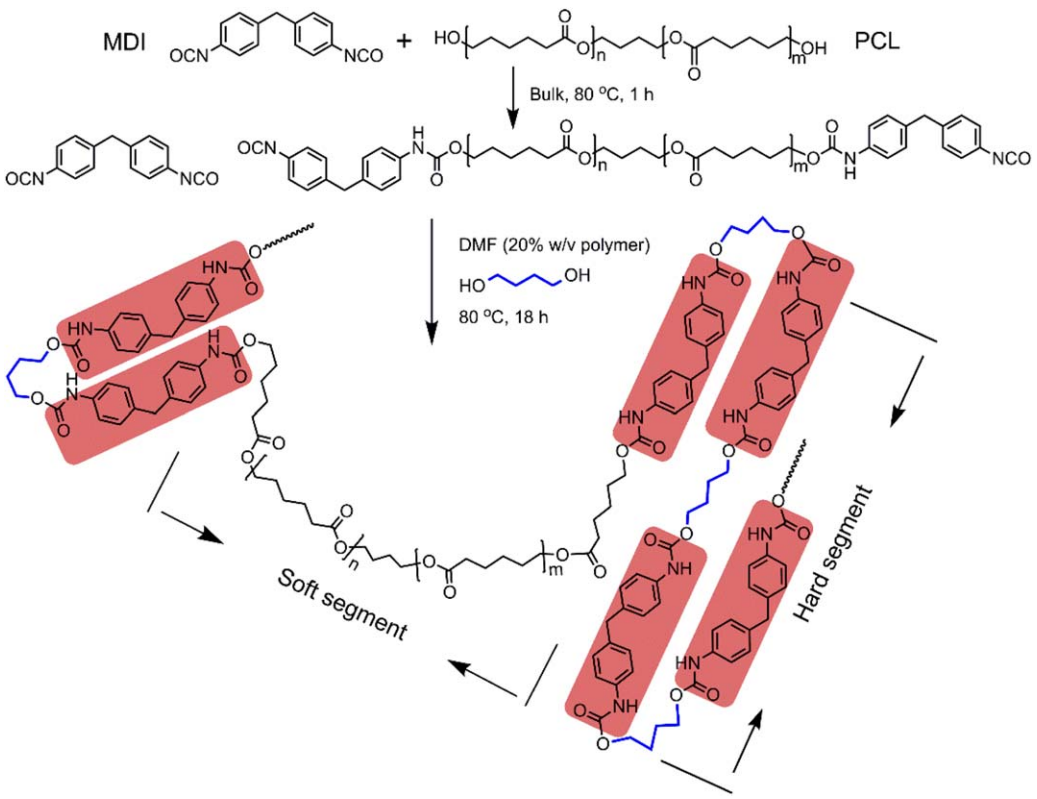

SCHEME 2 Synthesis scheme for ε-polycaprolactone-based polyurethanes. [Color figure can be viewed in the online issue, which is available at wileyonlinelibrary.com.]

length scales. In AFM studies the PeakForce QNM mode was used to quantitatively evaluate mechanical and adherence properties of the samples, that is, elastic moduli and adhesion, by means of collecting force-distance curves and applying a contact mechanics model (DMT, see Ref. 38). Additionally, we focused on the effect of composition on morphology and the formation of physical crosslinks, soft and hard phase crystallization and their morphological interplay. The results of this study allowed us to draw conclusions regarding molecular structure and structure–property relationships in the chosen class of PUs.

As a model system we studied PUs synthesized from 4,4'-methylenebis(phenyl isocyanate) (MDI), 1,4-butanediol (BD) and ε-polycaprolactone diol (PCL) with a constant stoichiometric ratio of the isocyanate and hydroxyl groups, but by systematically varying the stoichiometric ratio of polymer diol to total diol. These systems were found by Kim and Lee as exhibiting excellent shape memory effects.[39] Our syntheses were carried out in solution and the polymers were melt processed.

EXPERIMENTAL

Materials and Polyurethane Synthesis

The series of polyurethane elastomers with the ratio of PCL ($M_w = 2000$ g mol^{-1}, Sigma-Aldrich) and BD (Alfa Aesar) content ranging from 0.0 to 1.0 was synthesized according to the following procedure (based on a product yield of 30 g). Oven dried glassware was placed in a nitrogen-filled glove box and allowed to cool to room temperature while oxygen and moisture were purged under a flow of dry nitrogen for 30 min. MDI (Sigma-Aldrich) was weighed and transferred to a 24/40 joint size 3-neck flask. Molten PCL was weighed into an addition funnel. The reaction vessel was fitted with a mechanical stir shaft, a rubber septum and the addition funnel containing the polyol and then removed from the glove box. The stir shaft was attached to an overhead stir motor and the flask was immersed in an oil bath equilibrated at 80 °C. The molten PCL was added to the liquid MDI dropwise under moderate stirring. After 1 h of reaction time, the oil bath temperature was lowered to 50 °C and dry, distilled DMF (150 mL) was added to the flask by a double-tipped needle. BD was then added to the solution by syringe and the mixture was allowed to stir for an additional 18 h.

After completion (in MDI excess), the reaction was terminated by end-capping residual isocyanate groups with an excess of BD (1 mL). The polymer was precipitated from the reaction solution by pouring into a 5-fold excess of methanol or ethanol to yield a white solid or slightly yellow solid (the consistency varied with composition of the polymer). The synthesis scheme is diagrammed in Scheme 2.

Molecular sieves were activated by heating at 300 °C under vacuum at a base pressure ~27 mPa for 24 h. Silica gel was dried under vacuum at 120 °C for 2 h. N,N-dimethylformamide

(DMF) was dried over activated silica gel pellets, distilled over fresh powdered activated silica gel at reduced pressure, and stored over activated 0.4 nm molecular sieves until use. PCL was dried under vacuum at 100 °C for 3 h before use. For the hard segments BD was distilled under vacuum and stored over activated 0.4 nm molecular sieves. MDI flake was used without further purification.

A list of the PCL polymers prepared is provided in Table 1. In the table the NCO/OH value refers to the stoichiometric ratio of the isocyanate and hydroxyl groups, whereas the p(OH)/OH ratio refers to the amounts of OH in the soft segment polyol relative to the total OH content in the synthesis. As polyurethane synthesis can be considered a step-reaction polymerization, an equimolar ratio of the functional groups is required in order to achieve maximum molar mass.[8] Only a slight MDI excess was applied in order to compensate for the loss of isocyanate functionality due to side reactions. The hard segment (HS) content, as well as the average length of the hard segments, were estimated based on the initial concentration of the components according to the method described by Peebles,[40] assuming complete conversion, equimolar stoichiometry and an equal reactivity of the isocyanate groups. Isocyanate groups connecting PCL units were considered as part of the soft segments.

TABLE 1 Specification for Polyurethane Elastomers

Sample name	NCO/OH [-]	p(OH)/OH [%]	HS content [wt %]	HS length [nm]
C0	1.01	0	100.0	-
C10	1.01	10	53.4	19.8
C20	1.01	20	32.2	9.9
C30	1.01	30	20.3	6.6
C40	1.01	40	13.1	5.0
C50	1.01	50	8.3	4.0
C60	1.01	60	5.1	3.3
C70	1.01	70	3.0	2.8
C80	1.01	80	1.5	2.5
C90	1.01	90	0.6	2.2
C100	1.01	100	0.0	0.0

Sample Preparation (Microtome)

Structurally heterogeneous, multiphase-multicomponent polymer samples must be carefully prepared by microtoming for microscopic investigations.[41] Poor sample preparation approaches may expose bulk areas for microscopy analysis that are not representative of the bulk (concentration, appearance). At the cutting interface the PU components tend to relax to balance the interfacial forces originating in their multi-phase morphology. To reduce the impact of this possibility, one should cut the sample and investigate it immediately. For most mechanically compliant samples cutting at room temperature will induce additional stress in the sample and can lead to large surface roughness.

To avoid the above discussed situation, we cryo-microtomed (Ultracut EM-FCS, Leica, Germany) our samples. Specimens were sliced ($1 \times 2 \times 5$ mm^3), mounted onto a steel sample holder, and cooled with liquid nitrogen down to -125 °C. Two knives were employed for microtoming. A steel knife was used for a section of a nominal 2 μm thickness with a cutting speed of 2 mm s^{-1}. After the quality of this section was confirmed optically, a sharp glass knife at a 45 cutting angle was used for final surface cutting at a nominal 70 nm thickness with a cutting speed of 0.4 mm s^{-1}. Following completion of this cutting, samples were glued to a magnetic sample holder using a two component epoxy adhesive and measured immediately by AFM after the glue dried (~1 h). Samples older than 24 h were cryo-microtomed again for additional AFM experiments, when needed.

Macroscopic Mechanical Characterization Methods

For macroscopic mechanical characterization 1 mm thick polyurethane sheets were prepared by compression molding at 215 °C using a DAKE 50 ton lab press (model 944250-2), applying 3 min preheating with frequent degassing followed by 2 min pressing at a force of 200 kN (equivalent with a pressure of 5 MPa). Cooling the mold to room temperature typically took 10 min. The typical dimensions of the measured specimens were $7 \times 5 \times 1$ mm.

Dynamic mechanical analysis (DMA) was performed in the tension mode, at 1 Hz frequency, with the amplitude changing linearly between 10 and 100 μm, in the temperature range of -100 to 250 °C, using a TA instruments DMA Q800 apparatus.

Static mechanical properties were characterized by tensile testing on standard ASTM-D1708 micro-tensile specimens with a thickness of 1 mm, using an Instron 5565 apparatus, with 18 to 20 mm gauge length. The values of the Young's moduli, E, were determined at 0.5 mm min^{-1} crosshead speed between 0.5 and 1% deformation.

Thermal Characteristics

Thermal characterization of the polyurethane samples was carried out by DSC scanning from -90 to 220 °C in nitrogen at a heating/cooling rate of 10 °C min^{-1}, using a TA Instruments DSC Q2000 instrument. Glass transition temperatures of the soft segments were determined from the DSC curves as the inflection point of the endothermic change in the heat flux signal during the first heating run (not shown). The degree of crystallinity in the PCL phase, C_{PCL}, was obtained using the following equation

$$C_{PCL}\ (\%) = \left(\frac{\Delta H_{m,PCL}}{\Delta H^0_{m,PCL}}\right) 100 \quad (1)$$

where $\Delta H_{m,PCL}$ is the heat of fusion of PCL in the polyurethane samples investigated, determined by integrating the melting peak obtained in the first DSC heating scan, while $\Delta H^0_{m,PCL}$ is the heat of fusion of a fully crystalline PCL homopolymer (139.3 J g^{-1}).[42] For an example, see Supporting Information Figure S1.

Quantitative Mapping of Young's Modulus and Adhesion Force by AFM

Imaging Conditions

Samples were measured in the PeakForce QNM mode by a Multimode 8 AFM retrofitted with the NanoScope V controller (Bruker). In the PeakForce QNM mode information about the tip-sample interactions is obtained and evaluated in real-time by collecting force-distance curves and their simultaneous processing. The AFM probe cantilever was vertically oscillated at 2 kHz, which is far from its resonance frequency and helps to avoid a filtering effect.[43] The working distance (peak-force amplitude) was set to 150 nm. The force-distance curves were captured each time the AFM tip tapped on the sample surface, that is, at each pixel. Due to the geometry of the tip-sample interactions the imaging technique works with almost no lateral forces, which enhances sample phase identification and reduces sample and tip wear. Details of the scanning conditions are provided in the Supporting Information.

Contact Mechanics Model

Values of the Young's modulus can be obtained by measuring the deformation under an applied load. In AFM this is achieved by studying the indentation of an AFM tip.[16] For quantitative results, values of the Young's moduli were determined with reference to a material of a known DMT elastic modulus (see: System calibration). Details of the contact mechanics theory used and remarks about the conditions are summarized in the Supporting Information.

System Calibration

We used the "relative method" to measure Young's modulus in the PeakForce QNM mode to be able to perform an advanced real-time data analysis and reduce the propagation of errors.[44] The "relative method" is based on a simplified DMT formalism given in Supporting Information eq S6. In the "relative method" each cantilever/tip combination needs to be calibrated to obtain (quantified) elastic modulus values of unknown samples. Details of the "relative method" method and the discussion about measuring errors can be found in the Supporting Information.

As reference sample, we used polydimethylsiloxane (PDMS) gel 150 μm films with known Young's modulus of (3.5 ± 0.5) MPa (provided by Bruker).[44,45] A broad range of expected E values in our polyurethane samples required a large accessible range of the cantilever's deflection. Therefore, we double-checked our calibration with another reference sample of higher rigidity, that is, a cryo-microtomed bead of high density polyethylene, HDPE (0.95 kg m^{-3}, $M_w \sim 1.25 \cdot 10^5$ g mol^{-1}, Sigma-Aldrich). HDPE has E values, typically from 0.6 GPa to 1.4 GPa,[23,46] but in some literature the E range is even broader.[47] An excellent agreement was obtained between the measured E and the literature. In our HDPE reference sample E values varied from ~0.35 GPa to ~1.6 GPa, depending on the particular area (amorphous, semicrystalline, crystalline) hit by the tip, with an average $E = 713$ MPa for the entire AFM image (elasticity map). Bartczak and Kozanecki[47] showed that HDPE, with its macroscopic Young's modulus of around 700 MPa, contains approximately 40% of the amorphous and 60% of the crystalline phase. This proportion is in agreement with the phase contribution in our AFM elasticity maps (not shown). We also clearly observed two different phases (amorphous and crystallized with typical stacked lamellar morphology[48]) with their narrow transition areas (semicrystalline).

RESULTS AND DISCUSSION

Dynamic Mechanical Analysis and Glass Transition Temperature

The thermomechanical properties of the polymers were analyzed by dynamic mechanical analysis. Figure 1 presents the DMA curves of the C20, C40, and C80 samples. The lowest temperature transition in all cases is attributed to the glass transition of the soft segments ($T_{g,\ PCL}$) at around −35 °C, indicated by a drop in the storage modulus (E') signal accompanied by peaks in the loss modulus (E'') and the loss factor ($\tan\delta$). The subsequent decrease at around 50 °C in the moduli signals can be assigned to the melting temperature of the soft segments ($T_{m,\ PCL}$). At a higher temperature [~125 °C in Fig. 1(a,b)] the polymer starts to flow, as the steep increase of the $\tan\delta$ signal indicates. Above its flow temperature (T_f) the material shows viscous, liquid-like mechanical behavior, which also means the end of the measurement, as the sample reaches the maximum elongation enabled by the device. At higher PCL contents, as in the case of the C80 sample [Fig. 1(c)], the melting of the crystalline part coincides with T_f, that is, as the PCL matrix melts, the whole polymer starts to flow. Above ~8 wt % of HS content [see Table 1 for samples C40 and C50 as well as Fig. 1(b)], however, the polyurethanes still exhibit rubber-like mechanical behavior above 50 °C, although their moduli show a strong temperature dependence. Thus, we can distinguish between $T_{m,\ PCL}$ and T_f transitions. The latter increases with increasing the amount of HS in the polymer, indicating the formation of physical crosslinks due to a phase separated morphology (e.g., C20).

The composition dependence of the glass transition of the soft phase presented in Figure 2 provides more insight into the phase morphology of the polyurethanes studied here. Compared to the PCL-based PU without hard segments (C100), $T_{g,\ PCL}$ at first increases with increasing hard segment content (i.e., decreasing p(OH)/OH ratio), due to the presence of dissolved, rigid hard segments in the soft phase. The value of the glass transition temperature reaches its maximum below the critical HS concentration required to phase separation (5.1 wt %, C60). Further increasing the concentration of HS results in a drop in $T_{g,\ PCL}$ (~12 °C between C60 and C50), indicating the appearance of a distinct hard phase. Thus despite the larger amount of hard segments in the polymer there is a reduced percentage of hard segments in the soft phase. The continuous decrease of glass transition temperature with decreasing p(OH)/OH ratio suggests a gradual decrease of miscibility and greater phase

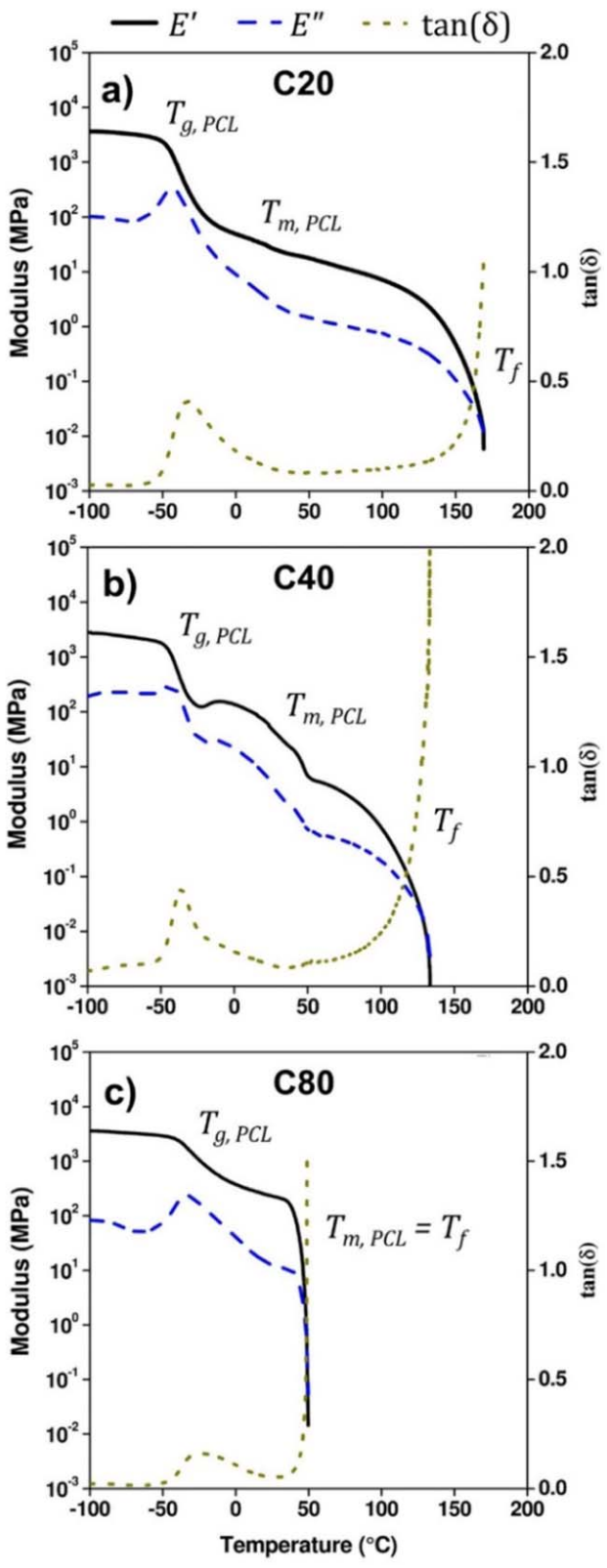

FIGURE 1 DMA spectra of the C20 (a), C40 (b) and C80 (c) sample. [Color figure can be viewed in the online issue, which is available at wileyonlinelibrary.com.]

separation in this composition range. The remarkably high $T_{g,\,PCL}$ of the sample with a p(OH)/OH ratio of 10% (C10), on the other hand, deserves special attention. At such a high hard segment content (53.4 wt %) the hard phase becomes the continuous matrix, or at least we are close to phase inversion, and a high degree of phase mixing takes place, increasing the glass transition temperature of the PCL phase.

Static Mechanical Tensile Testing

The Young's moduli of the polyurethanes obtained by tensile testing are presented in Figure 3. Since this characteristic is measured at low deformations (0.5–1%), far below the mechanical failure of the specimens, it is essentially determined by the composition and the properties of the components. Starting from lower p(OH)/OH ratios, the stiffness decreases rapidly with increasing soft segment content. As we noted above, in this composition range the polymer is supposed to have a phase separated morphology, thus the presence of a continuous matrix consisting almost exclusively of the soft PCL phase not surprisingly results in low modulus values. At higher soft segment contents (above 50% p(OH)/OH ratio), however, stiffness is considerably greater. This may be explained by phase mixing and the presence of rigid hard segments dissolved in the matrix. On the other hand, the modulus further increases with increasing p(OH)/OH ratio, despite the decreasing hard segment concentration. The explanation for this is that above 50% of p(OH)/OH ratio the PCL phase is able to crystallize, and the degree of crystallinity generally increases as more PCL is added to the composition. Stiffness in this region is mainly determined by this increased crystallinity of the polymer. It is worth noting, however, that the sample with a p(OH)/OH ratio of 90%

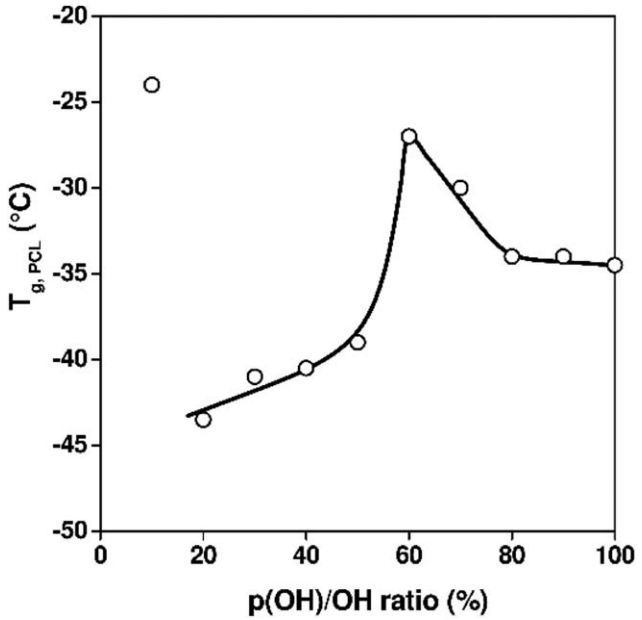

FIGURE 2 The glass transition temperature of the soft phase derived from the DMA spectra as a function of p(OH)/OH ratio. The line is a guide to the eye.

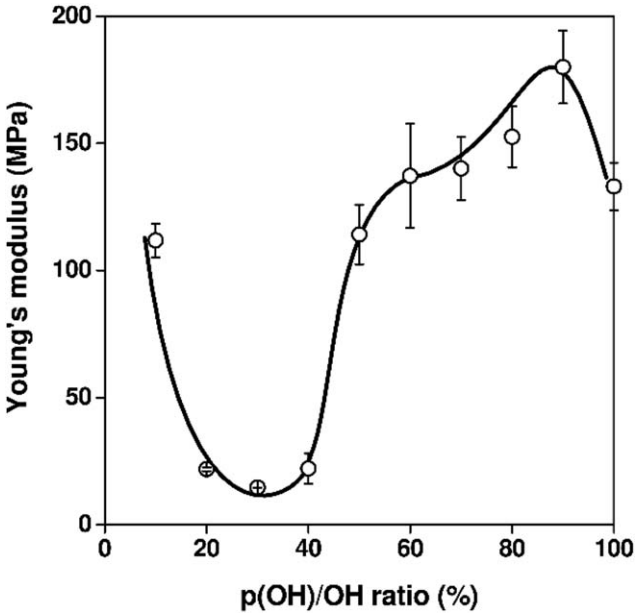

FIGURE 3 Young's modulus obtained by static mechanical testing as a function of p(OH)/OH ratio. The error bars indicate the standard deviation of mean. The line is a guide to the eye.

(sample C90) still has a higher modulus value than the homopolymer (sample C100). Both samples have a high degree of crystallinity (C90: $C_{PCL} = 43.3\%$, C100: $C_{PCL} = 40.2\%$), but in the case of C90 stiffness is further increased by the presence of dissolved hard segments in the PCL matrix.

AFM PeakForce

Topography and Morphology

Height and corresponding PeakForce error images of C20, C30, C40, C60, and C80 samples are shown in Figure 4. The image for sample C20 reveals a two component structure consisting of a: flat regions (soft phase) between elongated (up to about 3 μm in length) and high (locally up to about 200 nm) domains (hard segments) [Fig. 4(a)]. Small hard domains, approximately 250 nm in length and 30 nm in height, are present as well, but occur much less frequently. Significant phase separation can be observed in sample C20. The hard domains contain parallel whiskers [this feature is shown with high resolution in Fig. 7(a) and discussed later on]. The whiskers are highly ordered and directed. Each whisker has a rather fixed width of about 10–15 nm (see Fig. 7 as well) and varied length from about hundreds of nanometers up to some micrometers, as limited by the hard domain's length [Fig. 4(f)]. Schön et al. reported, for instance, on data regarding the width of approximately 20 nm and length from 30 to 200 nm for whiskers in poly(tetrahydrofurane)-based polyurethanes.[7] The elongated shape of the hard domains [Fig. 4(a,f)] is an intrinsic feature of the structure and is not related to microtoming; as the cryo-microtome cutting direction was "horizontal." On the contrary, the height of the domains may be influenced by the cryo-microtome cutting. We attribute the differences in the height of hard domains to the variation of the domain's rigidity (this later will be confirmed by AFM elastic modulus analysis). Similarly, the occurrence of flat regions in the image can be attributed to the soft phase. Possibly, at −125 °C hard domains and soft phase still reveal difference in

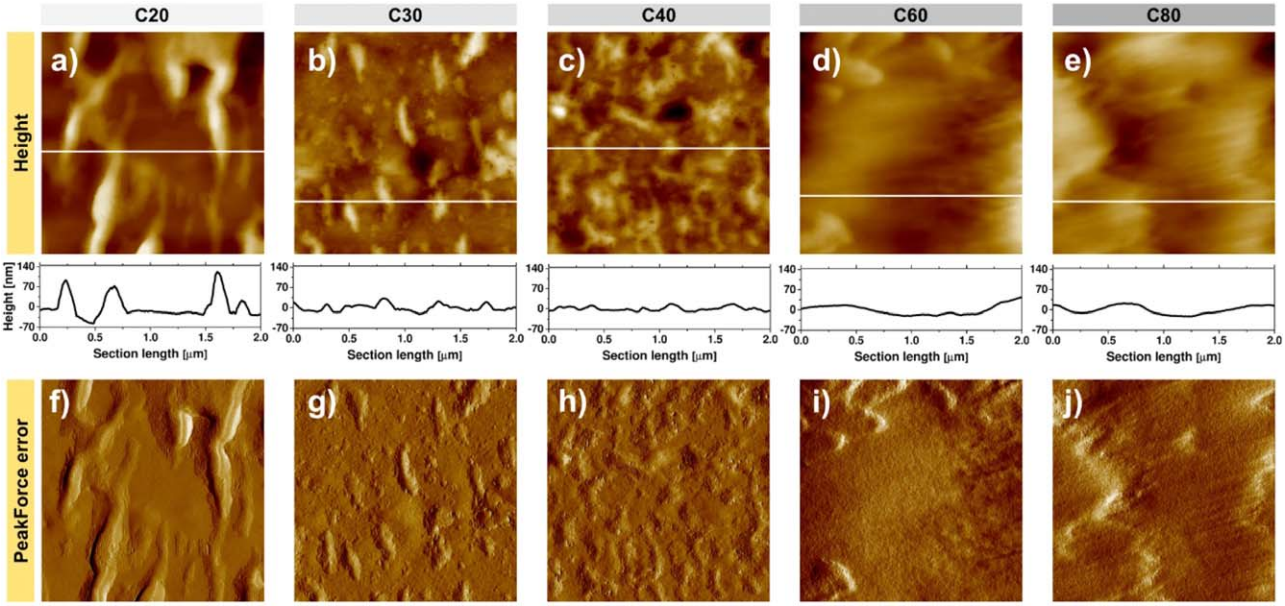

FIGURE 4 Height and corresponding PeakForce error images of samples C20, C30, C40, C60, and C80. The scan area is 2 × 2 μm^2. The height-profiles (height vs. section length) represent an overall height scale of the samples; height-profiles were taken along the white lines shown in the images. All height-profiles were adjusted to the same height scale to allow profile comparison. [Color figure can be viewed in the online issue, which is available at wileyonlinelibrary.com.]

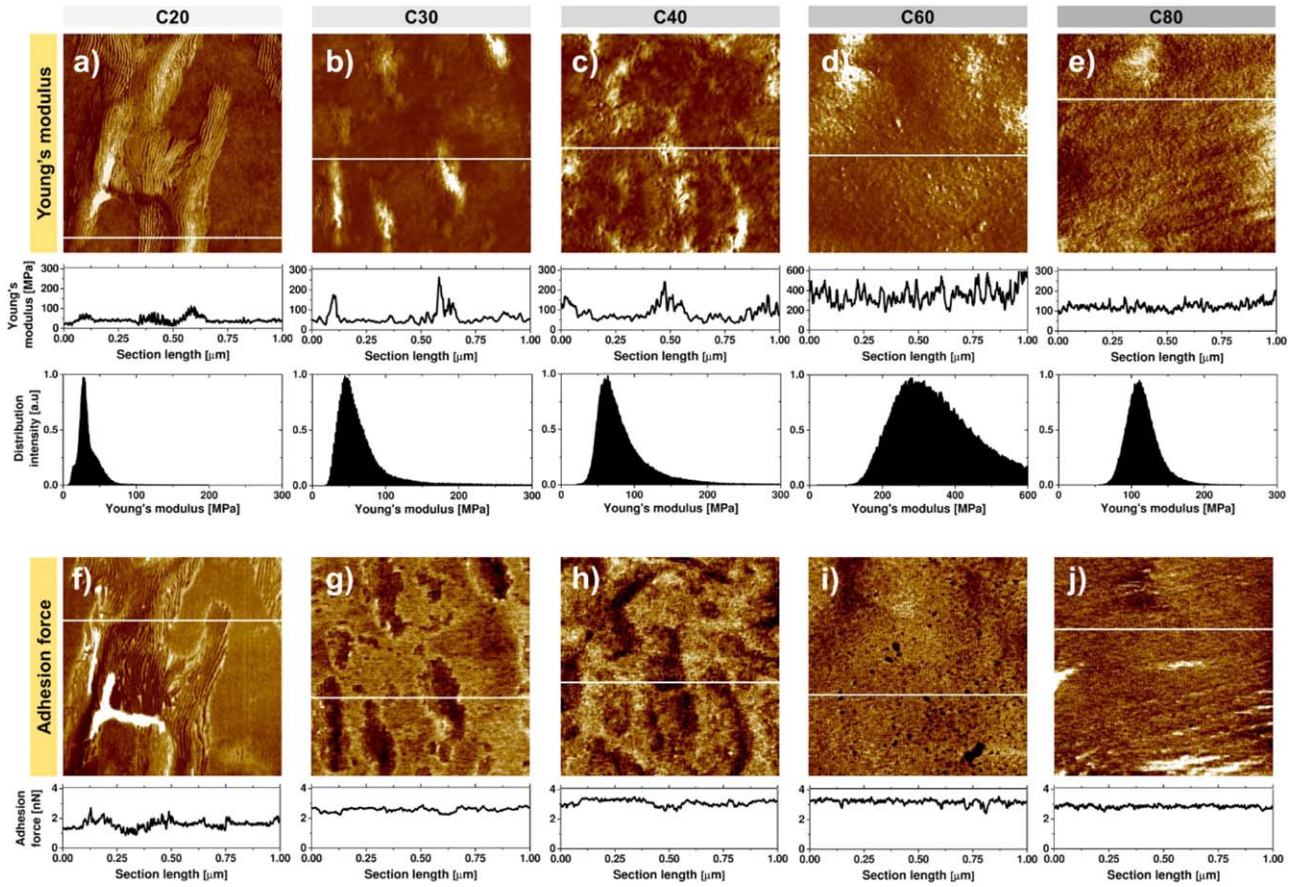

FIGURE 5 Young's modulus and corresponding adhesion force images of samples C20, C30, C40, C60, and C80. The scan area is 1 × 1 μm^2. The Young's modulus-profiles (Young's modulus vs. section length) and adhesion force-profiles (adhesion force vs. section length) were taken along the white lines. The corresponding distributions of Young's moduli are shown as histograms. [Color figure can be viewed in the online issue, which is available at wileyonlinelibrary.com.]

abrasion and mechanical compliance, the microtome knife removing the material in the two regions with different "efficiency."

Sample C30 shows significant differences compared to C20 [Fig. 4(b,g)]. The domains are smaller, both in lateral (up to about 400 nm) and vertical directions (up to about 50 nm). The volume of the hard domains is reduced, and thus they are better dispersed in the soft phase. While reducing the HS content in the polyurethane sample [C40, Fig. 4(c,h)], and thus the overall volume of the hard domains, the structure reveals a prominent increase in phase mixing (less phase separation). However, phase separation is still present at the submicron scale. The darkest areas in Figure 4(b,c) represent - probably - places from which the hard domains were pulled out by the microtome knife, which is most likely not the case for sample C20 due to the larger volume of the hard domains.

A p(OH)/OH ratio of 60% [sample C60, Fig. 4(d,i)] leads to a transition from the two component morphology into a homogenous and continuous morphology with mixed phases. Similar topography and morphology were observed in sample C80 as well [Fig. 4(e,j)].

We need to comment additionally on the topography in Figure 4(d,e). One can see the changes in the sample height-profile, however, they are not related to the presence of the hard domains, but are a result of cryo-microtome knife-carve artifacts, which are sometimes simply unfortunately present in the images.

Young's Modulus and Adhesion Force

The variation of the surface Young's moduli (DMT modulus maps) with the corresponding *E* value distribution and cross-section analysis are shown in Figure 5. As already shown in Figure 4(a), sample C20 reveals a two-phase (phase separated) character in its morphology, which can be quantified by high-resolution Young's moduli mapping [Fig. 5(a)]. *E* varies typically from about 25 MPa (soft phase) up to about 55 MPa (hard phase); locally even up to as much as 200 MPa (see Supporting Information Fig. S2). However, the presence of such highly rigid areas in sample C20 is rare, and therefore not seen in Figure 5(a) at the current distribution intensity scale. The Young's moduli distribution in Figure 5(a) shows a complex composition, that is, after analytical decomposition, it reveals three moduli peaks (see

Supporting Information Fig. S3). The central (narrow, the highest intensity, maximum at around 28 MPa) peak indicates the soft phase, the right peak (wide, moderate intensity, maximum at around 39 MPa) the whiskers in the hard domains, whereas the left peak (narrow, the lowest intensity, maximum at around 15 MPa) we attribute to soft areas between the whiskers. Similarly, broad E value distributions were obtained for other segmented polyurethane samples, for example, C30 and C40 [Fig. 5(b,c)], however, the distributions adopt mono-peak distribution with the log-normal envelope [the areas between the whiskers have modulus comparable to the soft phase "located" far away from the hard domains; see Fig. 7(b)].

As the HS content gradually decreases, the value of the Young's modulus monotonically increases (with an exception of C80). This is mostly due to the increased crystallinity of the soft phase and better dispersion of the HS in the soft phase (see additional discussion for Fig. 7). Sample C60, in particular, shows a remarkably high Young's modulus. This can be explained by the somewhat higher crystallinity of the soft phase in this sample (C_{PCL}: 48.6 vs. 40.6% in C80), and by the larger amount of rigid soft segments, compared to C80. The analysis of macroscopic properties based on tensile testing does not reflect the same tendency (see Fig. 3). The stiffness of the sample C60, however, has an exceptionally high standard deviation. The inhomogeneous structure of this polymer might play a role in the discrepancy between the results determined on a macro and mesoscales, respectively.

In the AFM experiments the local variation of adherence between the tip and sample is also measured pixel-by-pixel at the point of tapping. The corresponding adhesion force maps [Fig. 5(f–j)] confirm the above statements regarding the elasticity of the polyurethanes. The adhesion force values decrease when the AFM is retracted from the rigid area (small tip-sample contact area), but increase when the AFM is retracted from the mechanically compliant area (large tip-sample contact area); these differences are the greatest in sample C20 [Fig. 5(f)].

A discussion about the accuracy of the Young's modulus and adhesion force determination is provided in the Supporting Information.

Figure 6 shows a comparison of Young's moduli values obtained by AFM and DMA measurements, respectively, at room temperature (21 °C), as a function of p(OH)/OH ratio. For AFM data the E values correspond to the peak of the modulus distribution (Fig. 5) and for DMA they represent absolute values of the complex quantity which combines both real and imaginary DMA modulus components (data partly shown in Fig. 1). These two particularly different methods, both regarding the scale and methodology points of view, gave rather similar results. The largest dissimilarity can be related to fundamentally different averaging procedures. Neglecting the concrete E values and the accompanying errors in AFM (see error's discussion in the Supporting Information), both methods indicate analogous trends in elasticity, including significant E increases for sample C60. Even the bulk values obtained by tensile testing (Fig. 3) representing the bulk values obtained by the tensile testing partly coincide with the data shown in Figure 6. We note, however, that the DMA and static mechanical testing data cannot be strictly compared with AFM data due to the different deformation geometries and testing frequencies.[49] Nevertheless, they should reveal similarities.

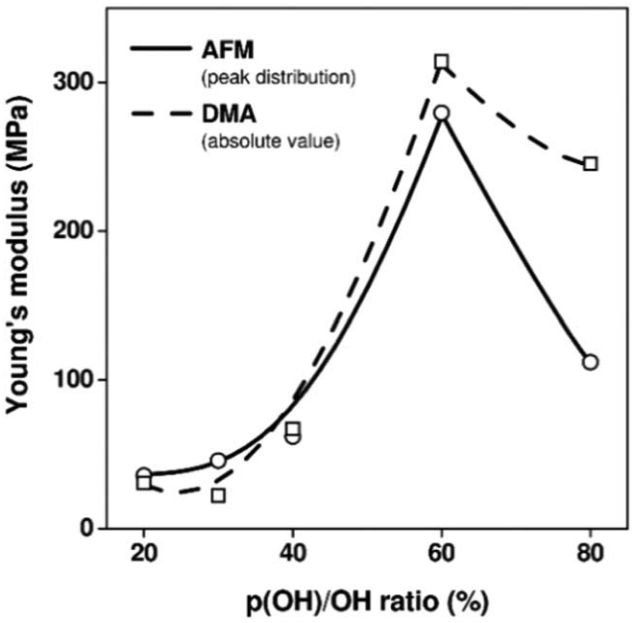

FIGURE 6 Comparison of Young's moduli obtained by AFM (measured at peak distribution; Fig. 5) and DMA (absolute value of the storage and loss modulus) measurements at 21 °C as a function of p(OH)/OH ratio (AFM: in circles; DMA: in squares). The lines are guides for the eye.

Macromolecular Structure–Property Relationships and Molecular Identification

In this section, we propose a structure based model for the studied polyurethanes consistent with the structure–property relationships already described. The images shown in Figure 7(a–c) represent high-resolution (150 × 150 nm^2) elasticity maps for samples C20, C40 and C80, respectively. From these images areas of 40 × 40 nm^2 (white square regions in Figure 7) have been selected to describe the model. The selected areas intentionally contain surfaces of high elasticity contrast (soft and hard phases).

We identify the polyurethane chain segments of different rigidity shown in Schemes 1 and 2, based on morphology and the corresponding Young's modulus in Figure 7 (model structure). Thus, we schematically marked the hard segments as red lines (MDI segments with the BD chain extenders). The hard segments are aligned in parallel stacks, resulting in the formation of whiskers. Due to the polydisperse nature of macromolecules, the length of the hard

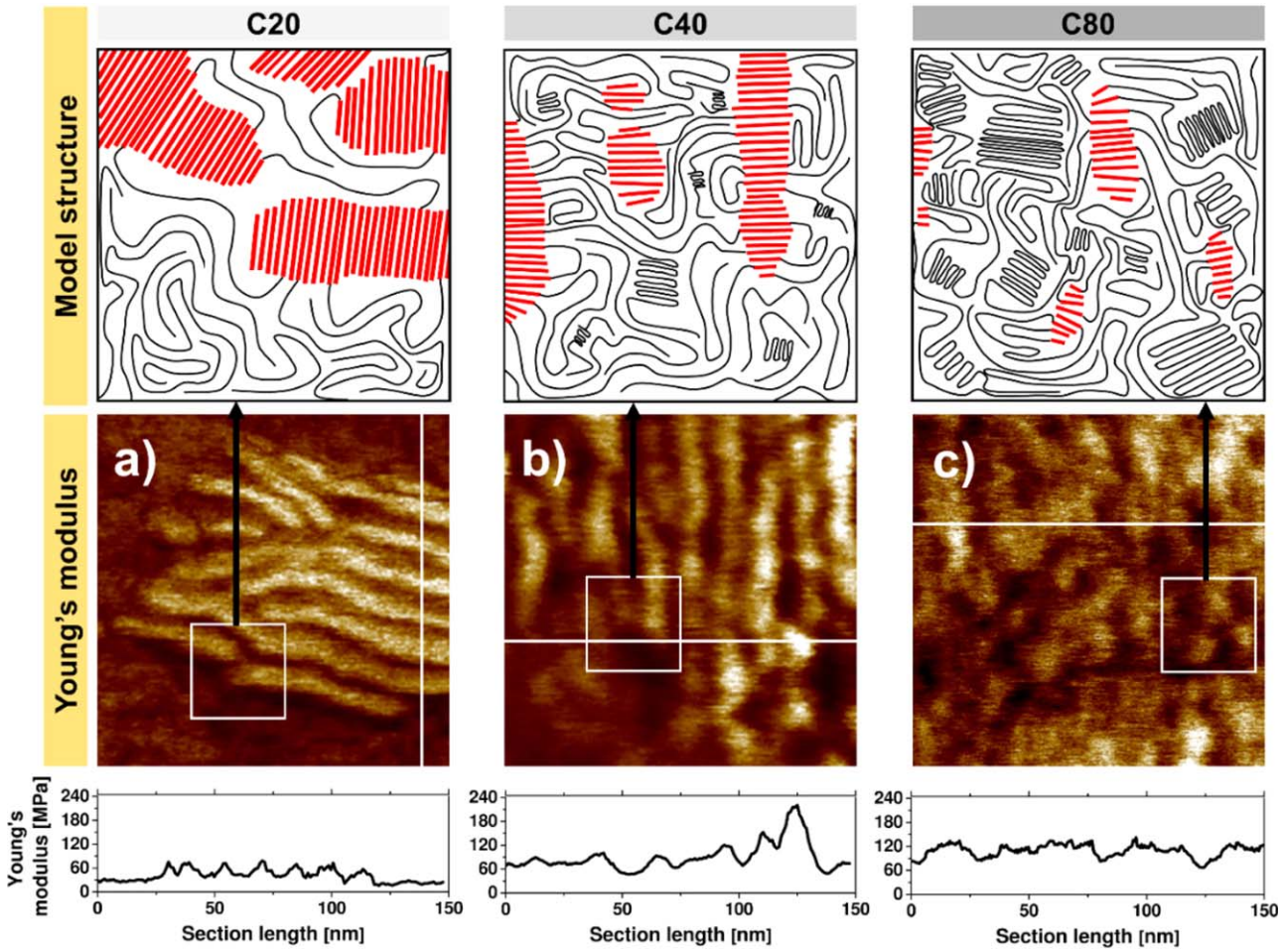

FIGURE 7 High resolution Young's modulus images of samples C20, C40, and C80 with their corresponding structural model. The scan area is 150 × 150 nm^2. White squares indicate areas with size of 40 × 40 nm^2 for which the structural model has been sketched. Wider, straight lines (red) indicate ordered MDI-BD segments (note that, to provide a clearance in the sketch, we do not show the chain extenders that lean out of the MDI-BD stack to be connected to a next stack); wider, straight lines (red) indicate PCL with eventual soft MDI segments (no chain extenders). The Young's modulus-profiles (Young's modulus vs. section length) were taken along the white lines shown in the images. [Color figure can be viewed in the online issue, which is available at wileyonlinelibrary.com.]

segments (straight lines), and thus the width of the whiskers varies.

For sample C20 [Fig. 7(a)], as already mentioned, the width of a single whisker is 10-15 nm (i.e., length of the straight lines). This perfectly matches with the estimated average HS length shown in Table 1 (~10 nm). The whiskers are highly ordered; this is evidence for strong interactions between the MDI segments, particularly due to H-bonding.[6,50] However, H-bonding alone cannot explain a relatively high variation in the *E* values obtained for whiskers, that is, from about 40 MPa [Fig. 5(a)] up to 200 MPa (Supporting Information Fig. S2). We speculate that this might be due to an interplay among the different intermolecular interactions in MDI segments: (1) hydrogen bonding between carbamoyl groups and carbonyl groups, (2) dipole–dipole interactions between carbonyl groups, and (3) induced dipole–dipole interactions between aromatic rings, as shown by Lee et al. to be typical for a sample with high HS content.[51] All these interactions provide a pseudo-crosslinked network structure among MDI-BD chains.[52] On the other hand, Bras et al. suggests that the driving force for the structure development, and thus mechanical properties, in polyurethanes, is the thermodynamics of phase separation (C20 is phase separated), rather than hydrogen bonding.[53] This could additionally explain the large variation in the Young's modulus values for sample C20.

An interesting result using PeakForce QNM was recently obtained by Fernandes-d'Arlas and Eceiza for homopolymer polyurethane based on 1,6-hexamethylene diisocyanate and BD.[25] The value of the elastic moduli was approximately 3.8 GPa. Such high elastic modulus values were explained by the authors as related to the high density of hydrogen-bonded carbonyls and high fraction of crystals with high packing density.

Despite the occurrence of highly ordered whiskers, this phase separation in sample C20 can explain the remarkable elasticity contrast [Fig. 7(a)]. Additionally, at such a low

p(OH)/OH ratio, the soft phase does not crystalize ($C_{PCL} = 0\%$), which also increases the contrast in the elasticity maps.

The areas between the whiskers in sample C20 require additional comment. As indicated above, an average Young's modulus in these areas was found to be lowered by a factor of approximately 2; from 28 to 15 MPa [distribution in Fig. 5(a)]. We attribute this to the decreased density of the PCL phase between the whiskers (corresponding PCL segments were shown in Figure 7(a) as black curved lines; see Scheme 1b as well). We think that the mobility of the soft segments within the hard domains is promoted by the poor alignment of the PCL chains between the whiskers, since this latter is restricted by the presence of highly ordered hard whiskers. This effect seems to be less prominent in the other phase-segregated polyurethanes (C30, C40); the smaller, less ordered whiskers probably allow the PCL chains align better inside the hard domains (among the whiskers), thus they are able to orientate in a way that results in more interactions among them, and in some cases might even lead to crystallization.

As the p(OH)/OH ratio increases [C40, Figs. 5(c) and 7(b)] physical crosslinks—present due the soft-hard phase separation—are reduced and more hard domains (but of a lower volume) are dissolved in the soft phase. Additionally, the PCL-based soft phase starts to crystallize (C40: $C_{PCL} = 10.8\%$); schematically showed in Figure 7(b) as more ordered black curves. This can explain two aspects: (i) a jump in the Young's modulus from about 28 MPa to about 60 MPa in the PCL-based soft phase apart from the hard domains [compare cross-sections for the soft phase in Fig. 7(a,b)], and (ii) high E values across the hard domains [maximum in the cross-section in Fig. 7(b)]. Regarding the point (ii), we assume that the presence of a partly crystallized PCL-based phase can largely enhance the overall rigidity of the whiskers. The structural order of the whiskers as well as the hard domains, on the other hand, seems to decrease. This is also confirmed by DSC measurements, as transition temperatures attributed to both the melting of the crystalline HS phase and the disruption of the H-bonding between the hard segments decrease with increasing p(OH)/OH ratio (data not shown). The decrease in the structural order of the whiskers is related to the reduced length of the HS (~5 nm, Table 1), and is shown as red lines with partly disordered parallel stacks in Figure 7(b,c).

Below the critical HS content required for phase separation (~10 wt %), for example, in the samples C60 and C80, the polyurethane surface reveals a continuous matrix with small and well dispersed whiskers in the PCL-based phase [C80, Fig. 7(c)]. Phase-isolated hard domains are no longer present, that is, the hard domains are completely dispersed in the soft phase. For samples C60 and C80 the soft phase can easily crystallize; C60: $C_{PCL} = 48.6\%$, C80: C_{PCL} 40.6%. Accordingly, the overall Young's modulus increases, but also does not vary much across the sample surface [compare the cross-section analysis in Fig. 5(c,e) or Fig. 7(b,c)], indicating similar mechanical compliance of the dissolved hard phase (whiskers) and the crystallized PCL-based phase. The width of the whiskers is much reduced (~2.5 nm, Table 1), thus creating a poor structural order. Due to this, whiskers cannot provide high rigidity, therefore, the value of Young's modulus (at a whisker) drops significantly.

CONCLUSIONS

The work presented represents additional insights in the field of PUs, using quantitative and high-resolution AFM nanomechanical mapping for unveiling structure–property relations in polycaprolactone based polyurethanes.

We have been motivated to study a series of PU samples to appoint material composition candidates for biomedical applications. Thus, we synthesized polyurethanes samples composed of MDI, BD, and PCL. The stoichiometric ratio of the isocyanate and hydroxyl groups was held constant, but the ratio of polymer diol to total diol, p(OH)/OH, was systematically varied (0 to 100%). The mechanical properties across the length scales were investigated by macro (DMA, tensile testing) and mesoscopic (AFM, QNM mode) mechanical testing.

We show that the nanoscale Young's modulus of polyurethane samples varies significantly across the sample surface depending on the chemical composition of the material. These variations are not "visible" in macroscopic mechanical testing, since they are "averaged" in the bulk. The phase-separated samples (C20–C50) show less variation in the values of the nanoscale Young's modulus compared to the phase-mixed C60 sample (the lowest molar mass and the highest $T_{g,\ PCL}$ in the series). In the case of sample C60, AFM revealed well dispersed hard domains in the soft phase reflecting variation in the structural order. On the other hand, DSC showed that the PCL-phase is almost half crystalline. These two issues imply not only a broad distribution, but also relatively high values of the nanoscale Young's modulus in sample C60, thereby rather moving that material composition away from most medical applications, which favor materials with low moduli. Specimens with higher PCL content (C70–C100) are also questionable for such purposes due to their low flow temperature above approx. 50 °C, and overall rigid character at room temperature, including relativity high $T_{g,\ PCL}$. The latter is also a cause for excluding sample C10 as material for biomedical applications. The phase-separated samples, C20–C40 (rather with an exception of C50), are much more promising for biomedical applications due to low Young's modulus, low $T_{g,\ PCL}$, and good overall material flexibility. A detailed physiochemical study of PCL-based PUs will be discussed in a forthcoming paper.

The structure–property relationships are essential in controlling the performance of the final material. The AFM Young's modulus maps shows a strict correlation among the size of the hard segments (also the width of whiskers), their structural order, soft-hard phase segregation, and the obtained

Young's modulus values. The width of the whiskers shows an excellent agreement with the estimated length of the hard segments calculated based on the initial concentration of the components. The AFM data also shows that the mechanical compliance of the (amorphous) soft PCL-phase can differ with respect to the areas "located" out of the hard domains and among the whiskers, indicating a variation in the alignment of the PCL chains.

ACKNOWLEDGMENTS

Support with Scheme 2 and valuable discussions with M.Sc. Kaihuan Zhang from the University of Twente are gratefully appreciated. H.G. also acknowledges Dr. Michel Klein Gunnewiek for his help with microtoming the specimens. Funding was provided by the MESA$^+$ Institute of Nanotechnolgy at the University of Twente. The US portion of the research was sponsored in part by the Bill and Melinda Gates Foundation "Grand Challenges" Initiative. The Gates Foundation is dedicated to helping people live healthier and more productive lives. Partial support also was provided by a grant from the Fidelity Charitable Foundation. These sponsors had no role in performing the research. The authors also acknowledge use of the outstanding analytical facilities of CAMCOR, the Center for Advanced Materials Characterization in Oregon located at the University of Oregon (camcor.uoregon.edu).

REFERENCES AND NOTES

1 P. Król, *Prog. Mater. Sci.* **2007**, *52*, 915–1015.

2 C. Prisacariu, In Polyurethane Elastomers: From Morphology to Mechanical Aspects; Prisacariu, C., Ed.; Springer Vienna: Vienna, **2011**, pp 23–60.

3 C.Hepburn. Polyurethane Elastomers; Springer: Netherlands, **1992**.

4 B. Imre, D. Bedo, A. Domján, P. Schön, G. J. Vancso, B. Pukánszky, *Eur. Polym. J.* **2013**, *49*, 3104–3113.

5 C. J. Paul, M. R. Gopinathan Nair, N. R. Neelakantan, P. Koshy, B. B. Idage, A. A. Bhelhekar, *Polymer* **1998**, *39*, 6861–6874.

6 K. Bagdi, K. Molnár, M. Kállay, P. Schön, J. G. Vancsó, B. Pukánszky, *Eur. Polym. J.* **2012**, *48*, 1854–1865.

7 P. Schön, K. Bagdi, K. Molnar, P. Markus, B. Pukanszky, G. Julius Vancso, *Eur. Polym. J.* **2011**, *47*, 692–698.

8 B. Pukánszky, Jr, K. Bagdi, Z. Tóvölgyi, J. Varga, L. Botz, S. Hudak, T. Dóczi, B. Pukánszky, *Eur. Polym. J.* **2008**, *44*, 2431–2438.

9 L. Rueda-Larraz, B. F. d'Arlas, A. Tercjak, A. Ribes, I. Mondragon, A. Eceiza. *Eur. Polym. J.* **2009**, *45*, 2096–2109.

10 H. Janik, M. Sienkiewicz, J. Kucinska-Lipka, In Handbook of Thermoset Plastics, 3rd ed.; Goodman, S. H., ed.; William Andrew Publishing: Boston, **2014**, pp 253–295.

11 W. Kang, J. O. Stoffer, *Polym. Prep.* **2000**, *41*, 1132–1133.

12 D. J. Liaw, *Angew. Makromol. Chem.* **1997**, *245*, 89–104.

13 E. Tocha, H. Janik, M. Dębowski, G. J. Vancso, *J. Macromol. Sci. Phys.* **2002**, *41*, 1291–1304.

14 G. Huang, H. Lu, *Mech. Time-Depend. Mater.* **2006**, *10*, 229–243.

15 B. Mailhot, K. Komvopoulos, B. Ward, Y. Tian, G. A. Somorjai, *J. Appl. Phys.* **2001**, *89*, 5712–5719.

16 H. J. Butt, B. Cappella, M. Kappl, *Surf. Sci. Rep.* **2005**, *59*, 1–152.

17 G. Binnig, C. F. Quate, C. Gerber, *Phys. Rev. Lett.* **1986**, *56*, 930–933.

18 D. Tranchida, S. Piccarolo, M. Soliman, *Macromolecules* **2006**, *39*, 4547–4556.

19 N. Chaiyut, T. Amornsakchai, S. Thanawan, *Polym. Test.* **2007**, *26*, 396–401.

20 L. Chopinet, C. Formosa, M. P. Rols, R. E. Duval, E. Dague, *Micron.* **2013**, *48*, 26–33.

21 O. Sahin, S. Magonov, C. Su, C. F. Quate, O. Solgaard, *Nat. Nanotechnol.* **2007**, *2*, 507–514.

22 M. E. Dokukin, I. Sokolov, *Langmuir* **2012**, *28*, 16060–16071.

23 T. J. Young, M. A. Monclus, T. L. Burnett, W. R. Broughton, S. L. Ogin, P. A. Smith, *Meas. Sci. Technol.* **2011**, *22*.

24 K. Sweers, K. van der Werf, M. Bennink, V. Subramaniam, *Nanoscale Res. Lett.* **2011**, *6*, X1–10.

25 B. Fernandez-d'Arlas, A. Eceiza, *J. Polym. Sci. B.* **2016**, *54*, 739–746.

26 R. J. Zdrahala, I. J. Zdrahala, *J. Biomater. Appl.* **1999**, *14*, 67–90.

27 G. A. Skarja, K. A. Woodhouse, *J. Appl. Polym. Sci.* **2000**, *75*, 1522–1534.

28 E. M. Maafi, F. Malek, L. Tighzert, *J. Appl. Polym. Sci.* **2010**, *115*, 3651–3658.

29 R. Seoane Rivero, P. Bilbao Solaguren, K. Gondra Zubieta, L. Peponi, A. Marcos-Fernández, *Express Polym. Lett.* **2016**, *10*, 84–95.

30 F. Li, J. Hou, W. Zhu, X. Zhang, M. Xu, X. Luo, D. Ma, B. K. Kim, *J. Appl. Polym. Sci.* **1996**, *62*, 631–638.

31 J. Kloss, M. Munaro, G. P. De Souza, J. V. Gulmine, S. H. Wang, S. Zawadzki, L. Akcelrud, *J Polym. Sci. Part A.* **2002**, *40*, 4117–4130.

32 R. K. Agrawal, L. T. Drzal, J. Adhes, *Sci. Technol.* **1995**, *9*, 1381–1400.

33 E. Ibarboure, A. Baron, E. Papon, J. Rodriguez-Hernandez, *Thin Solid Films* **2009**, *517*, 3281–3286.

34 S. Sartori, M. Boffito, P. Serafini, A. Caporale, A. Silvestri, E. Bernardi, M. P. Sassi, F. Boccafoschi, G. Ciardelli, *React. Funct. Polym.* **2013**, *73*, 1366–1376.

35 F. Shokrolahi, H. Yeganeh, *Iran. Polym. J.* **2014**, *23*, 505–512.

36 G. Oertel, L. Abele, Polyurethane Handbook: Chemistry, Raw Materials, Processing, Application, Properties; Hanser, Munich, **1994**.

37 D. MacOcinschi, D. Filip, S. Vlad, M. Cristea, M. Butnaru, *J. Mater. Sci.: Mater. Med.* **2009**, *20*, 1659–1668.

38 B. V. Derjaguin, V. M. Muller, Y. P. Toporov, *J. Colloid Interface Sci.* **1975**, *53*, 314–326.

39 B. K. Kim, S. Y. Lee, M. Xu, *Polymer* **1996**, *37*, 5781–5793.

40 L. H. Peebles. Jr, *Macromolecules* **1974**, *7*, 872–882.

41 L. C. Sawyer, D. T. Grubb, G. F. Meyers, Polymer microscopy, 3rd ed, **2008**.

42 V. Crescenzi, G. Manzini, G. Calzolari, C. Borri, *Eur. Polym. J.* **1972**, *8*, 449–463.

43 H. Schillers, I. Medalsy, S. Hu, A. L. Slade, J. E. Shaw, *J. Mol. Recognit.* **2016**, *29*, 95–101.

44 Bruker, **2011**.

45 Z. Wang, A. A. Volinsky, N. D. Gallant, *J. Appl. Polym. Sci.* **2014**, *131*, 41050.

46 Springer Handbook of Condensed Matter and Materials Data; Springer-Verlag: Berlin, Heidelberg, **2005**.

47 Z. Bartczak, M. Kozanecki, *Polymer* **2005**, *46*, 8210–8221.

48 H. Zhou, G. L. Wilkes, *Polymer* **1997**, *38*, 5735–5747.

49 F. Chambon, Z. S. Petrovic, W. J. MacKnight, H. H. Winter, *Macromolecules* **1986**, *19*, 2146–2149.

50 C. Zhang, J. Hu, S. Chen, F. Ji, *J. Mol. Model.* **2010**, *16*, 1391–1399.

51 B. S. Lee, B. C. Chun, Y. C. Chung, K. I. Sul, J. W. Cho, *Macromolecules* **2001**, *34*, 6431–6437.

52 M. Rogulska, W. Podkościelny, A. Kultys, S. Pikus, E. Poździk, *Eur. Polym. J.* **2006**, *42*, 1786–1797.

53 W. Bras, G. E. Derbyshire, D. Bogg, J. Cooke, M. J. Elwell, B. U. Komanschek, S. Naylor, A. J. Ryan, *Science* **1995**, *267*, 996–999.